Picosecond damage studies at 0.5 and 1 μm

M. J. Soileau
William E. Williams
Eric W. Van Stryland
Thomas F. Boggess
Arthur L. Smirl
North Texas State University
Department of Physics
Center for Applied Quantum Electronics
P.O. Box 5368
Denton, Texas 76203

Abstract. The laser-induced damage (LID) thresholds of fused silica and single crystal NaCl were studied at wavelengths of 0.5 and 1 μm for pulses as short as 4 ps for a variety of focal spot sizes. The problem of sample-to-sample variation was minimized by performing parametric studies on a single sample at a time. Beam distortion measurements and polarization dependence studies of the LID thresholds demonstrate that the contribution of self-focusing to the LID measurements in this work was negligible. The damage threshold field E_B was found to increase as the pulsewidth was decreased in both materials at both wavelengths. The strongest pulsewidth dependence observed was approximately an inverse square root proportionality observed in NaCl at 1 μm for pulses shorter than 10 ps. For conditions of equal pulsewidth and the same focal spot size, E_B was less at 0.5 μm than at 1 μm for both materials.

Keywords: laser damage in materials; picosecond pulses; fused silica; NaCl; avalanche breakdown.

Optical Engineering 22(4), 424-430 (July/August 1983).

CONTENTS

1. Introduction
2. Experiment
3. Self-focusing considerations
4. Experimental results and discussions
5. Summary
6. Acknowledgments
7. References

1. INTRODUCTION

The problem of bulk laser-induced damage (LID) in nominally transparent materials has been the subject of extensive investigation.[1] However, after more than 15 years of study, bulk laser-induced damage is still not well understood. A major obstacle to developing models for such damage in highly transparent materials is the lack of a consistent data base for the dependence of LID on such basic parameters as laser wavelength and pulsewidth. The problems of sample-to-sample variations and the complex interdependence of the damage thresholds on laser frequency, pulsewidth, and focal conditions[2] make the interpretation of isolated data points difficult.

We have tried to minimize these problems by studying LID as a function of wavelength and pulsewidth for a variety of focal conditions on a given sample. In Ref. 2 the LID thresholds of a sample of fused SiO_2 and a single crystal NaCl sample were studied at 1.06 μm as a function of pulsewidth for pulses ranging from 40 ps to 31 ns using a variety of focal conditions. In that work we found that the laser-induced breakdown threshold field E_B (i.e., the rms field corresponding to the LID threshold peak on-axis irradiance) was only weakly dependent on the laser pulsewidth. We found that, for the range of parameters used, we could fit all the data in Ref. 2 to the following empirical relationship:

$$E_B = A/[t_p^{1/4}\omega_o^4] + B \ , \qquad (1)$$

where A and B are constants for a given sample, t_p is the laser pulsewidth, and ω_o is the laser focal spot radius. In the present work, we find that this relationship breaks down for pulses shorter than 10 ps.

Here we extend the pulsewidth dependence studies at a wavelength of 1 μm to pulses as short as 4 ps, and we study the LID characteristics of fused SiO_2 and single crystal NaCl at 0.53 μm for pulsewidths in the 20 to 200 ps range. We find that the empirical relationship given by Eq. (1) no longer holds for laser pulses shorter than 10 ps. For the shortest pulses (4 to 10 ps), E_B varied as approximately the inverse third root of the pulsewidth in SiO_2 and as approximately the inverse square root of the pulsewidth in NaCl for all the focal conditions studied.

For conditions of equal pulsewidth and the same focal spot size, E_B was less at 0.53 μm than at 1.06 μm for both materials for pulsewidths in the 40 to 200 ps range. This result is contrary to the predictions of a simple avalanche breakdown model. Also, the observed dependence, while in the right direction, is much too weak for a strictly multiphoton process. A multiphoton-initiated avalanche breakdown process[2] is a possible explanation for the observed wavelength dependence.

In addition, by carefully studying the polarization dependence of LID and by measuring the distortion of the transmitted beams, we show that the contribution of self-focusing to LID in our experiments is much less than has been assumed by other workers. In fact, for certain focal conditions we demonstrate that the effects of self-focusing are negligible.

2. EXPERIMENT

The lasers used in this study were a mode-locked Nd:YAG oscillator-amplifier system and a mode-locked Nd:glass oscillator system, which have been described elsewhere.[2,3] The YAG laser was operated at 1.06 μm and the glass at 1.05 μm. In each case a single pulse of measured Gaussian spatial distribution was switched out of the mode-locked train and amplified. The pulsewidth of the Nd:YAG laser was varied from 40 to 200 ps (FWHM) by selecting various étalons as the output coupler of the oscillator. The glass laser pulsewidth varied from 4 to 10 ps (FWHM). The pulsewidth and energy of each pulse were monitored. The width of each pulse was determined by monitoring the ratio of the energy in the second harmonic pro-

Invited Paper LD-106 received Dec. 29, 1982; revised manuscript received Mar. 3, 1983; accepted for publication Mar. 7, 1983; received by Managing Editor Mar. 21, 1983. A preliminary report of this work was presented at the Fourteenth Annual Symposium on Optical Materials for High Power Lasers, National Bureau of Standards, Boulder, Colorado, Nov. 15-17, 1982.
© 1983 Society of Photo-Optical Instrumentation Engineers.

duced in a $LiIO_3$ crystal to the square of the energy in the fundamental. A more detailed description of energy and pulsewidth measurement is given in Ref. 2.

A temperature-tuned CD*A crystal was used with the Nd:YAG laser to produce pulses at 0.53 μm. Care was taken to filter any residual 1.06 μm radiation from the 0.53 μm beam. The energy in the fundamental pulses at 1.06 μm was kept below values that would produce saturation effects in the spatial profile of the second harmonic. Two-dimensional scans of the 0.53 μm beam with an optical multichannel analyzer (OMA) verified the absence of saturation effects and the Gaussian spatial profile of the 0.53 μm beam. Such vidicon scans of the spatial beam profile showed that the shot-to-shot variation in the beamwidth was less than our detection resolution limit of approximately 1%. Second-order autocorrelation measurements of the 0.53 μm pulses and light-by-light scattering measurements in a $LiIO_3$ crystal[4] indicated that the 0.53 μm pulsewidth scaled as the 1.06 μm pulsewidth divided by $\sqrt{2}$. This scale factor was used to compute the 0.53 μm pulsewidths from the measured 1.06 μm pulsewidths.

The laser beam was focused into the bulk of the sample using single element "best form" lenses designed for minimum spherical aberrations. Three lenses of focal lengths 37 mm, 75 mm, and 150 mm were used at various distances from the beam waist to produce the focal spot radii for these experiments. The lowest f-number condition used in these experiments was f/10.3. In each case, the beam diameter was kept below maximum values necessary to ensure diffraction-limited performance. Aberrations caused by focusing through the planar surfaces of the samples were calculated to cause an error in the field of less than 0.1% for the worst case. The output energy of the CD*A crystal was monitored continually using a sensitive photodiode peak-and-hold detector absolutely calibrated with respect to a pyroelectric energy detector. Transmission through the sample was monitored by another peak-and-hold detector.

In some cases the transmission detector was replaced by a vidicon tube used in conjunction with an optical multichannel analyzer to scan the transmitted beam profile. Such scans were made at the damage threshold irradiance and for irradiance levels ten times below the damage threshold. In this way, a total time integrated beam distortion occurring at the beam waist of the order of λ/5 could be detected.

The short pulsewidth data (4 to 9 ps) were taken on the same samples using a microprocessor-controlled Nd:glass oscillator system operating at a laser wavelength of 1.05 μm.[3] This system produced single pulses of measured Gaussian spatial profile. Shot-to-shot energy fluctuations were determined to be ~20%. The same focusing lenses were used as with the 0.53 μm measurements. Beam scans as a function of distance from the laser were employed to determine the beam divergence (0.40 mrad) and the position and size of the output beam waist. This information and the lens focal length were then used to calculate the beam waist at the lens focus. Energy on target was varied using a calibrated Glan polarizer. The procedures for measuring and continuously monitoring both pulsewidth and energy are identical to those described previously with the Nd:YAG laser system.[2]

The breakdown threshold for a given pulsewidth was taken to be that irradiance which produced damage 50% of the time. Each site was irradiated only once. Damage was defined as the appearance of a visible flash in the bulk of the sample or by the observation of forward scattered light from a coaxial HeNe laser as viewed through a ten-power long-working distance microscope. The microscope also was used to verify that damage had occurred at the beam focus and was not due to inclusions. For 0.53 μm damage, the appearance of 0.53 μm scattered radiation and HeNe scattered light occurred simultaneously for both SiO_2 and NaCl. In the cases of the 4 to 9 ps data, for both SiO_2 and NaCl, there was a small range of incident energies where damage had occurred as determined from scattered HeNe radiation, but no flash was observed. N-on-1 experiments (multiple shot irradiation at the same sample site), conducted at both wavelengths, indicate no change in the breakdown threshold when compared to the 1-on-1 experiments (only one irradiation per sample site).

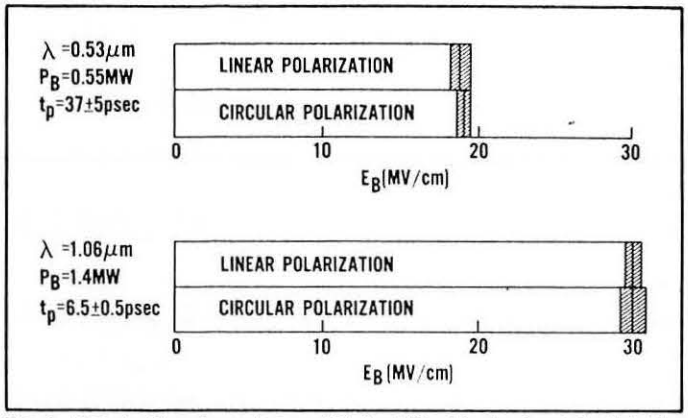

Fig. 1. Polarization dependence of E_B for SiO_2. The horizontal axis is E_B, the rms breakdown field corresponding to the peak on-axis irradiance at damage. P_B is the breakdown threshold power. Note the lack of polarization dependence for both wavelengths. The cross-hatched portions shown above are the relative uncertainties of the thresholds using the procedure given in Ref. 15.

3. SELF-FOCUSING CONSIDERATIONS

In order to produce laser-induced damage in the bulk of a highly transparent material, one must tightly focus the light into the material. Since the beam propagates through the material, one must consider self-induced lensing effects (i.e., self-focusing) on the results of bulk damage measurements, particularly when the power required to induce damage is of the order of the predicted critical power for self-focusing. Therefore, before any analysis of damage data can begin, one needs to devise tests which will verify the presence, or absence, of self-focusing effects.

One such test is to examine the polarization dependence of the LID threshold. Self-focusing theory predicts,[5–8] and experiments confirm,[6–10] that the critical power for self-focusing is *lower* for linearly polarized light compared to that for circularly polarized light. In Fig. 1 we present the results of polarization-dependent studies for a sample of fused quartz at laser wavelengths of 0.53 μm and 1.06 μm. The breakdown thresholds are given in terms of the rms electric field, in MV/cm, corresponding to the peak on-axis irradiance producing damage. In both cases we used the shortest pulses available to us, which corresponded to the highest input power for the given focal spot radius of 5 μm. All spot radii are quoted as half-widths at the e^{-2} point down from the maximum irradiance (HW $1/e^2$ M). As can be seen, the breakdown field for linear polarization equals that for circular polarization. In both materials no polarization dependence was observed for pulses between 4 to 9 ps (FWHM) at 1.05 μm even for the largest spot size used in this study. Similar results were obtained in measurements on a NaCl sample at a 0.53 μm laser wavelength. Thus, for the focal conditions used, we observed no polarization dependence of the breakdown thresholds for either fused quartz or NaCl.

Another independent test for the presence of self-focusing is to examine the beam spatial profile after transmission through the sample for irradiance levels far below and near the damage threshold. In Fig. 2 we show two vidicon traces taken in the far field through the center of the 0.53 μm beam after transmission through the fused quartz sample. The focal spot radius (HW $1/e^2$ M) at the beam waist for this configuration, in the absence of self-focusing, is approximately 7 μm. The solid trace was taken near the damage threshold. The dashed trace was taken at an irradiance level approximately ten times below the damage threshold. Filters were placed in front of the vidicon to adjust the irradiance at the vidicon surface to the same value in both traces in order to minimize any problems in detector nonlinearity. Inspection of Fig. 2 shows no detectable beam distortion for input powers approximately equal to the damage threshold power. Scans conducted for a focal spot size of 3.4 μm also show no distortions.

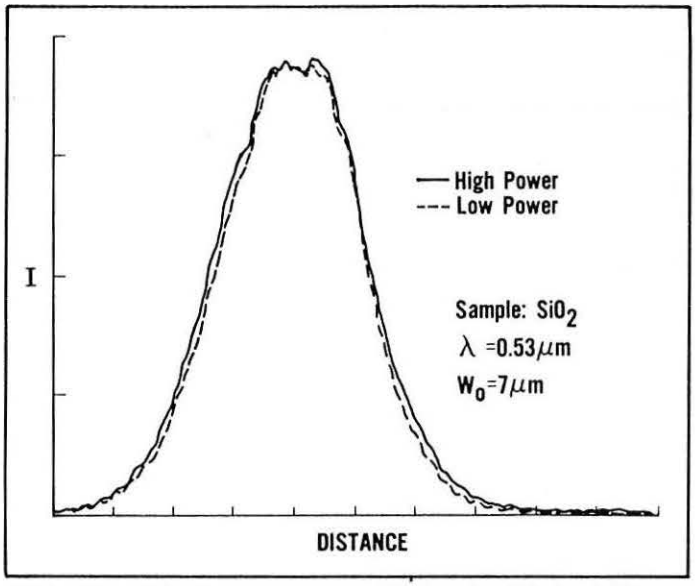

Fig. 2. Beam distortion measurements. This is a plot of the far-field beam profile of the 0.53 μm beam after propagation through the SiO_2 sample. The quantity $w_o = 7$ μm is the focal spot radius inside the sample calculated using linear Gaussian optics. The curve labeled "high power" was taken with the input power at the damage threshold level, and the one labeled "low power" was for input power approximately equal to one-tenth the damage threshold power. The noise in the above plots is instrumental.

The authors are aware that the technique just described monitors the time-integrated beam spatial profile; however, this technique is sensitive to a $\lambda/5$ distortion in the total time-integrated profile and has proven to be a sensitive technique for monitoring the onset of self-defocusing in solids.[11] These measurements, when taken together with the polarization experiments described above, indicate that self-focusing effects were not important for the geometries used in these experiments. However, the reader should be aware that in other experimental geometries (i.e., less tightly focused beams) self-focusing effects can be important. In fact, preliminary measurements in SiO_2 at 0.53 μm indicate that for a 14 μm focal spot radius the far field beam radii for irradiance at the damage threshold differ from those at low irradiance levels by approximately 28% (indicating that self-focusing has taken place). For that same focal geometry, the ratio of the LID threshold for circularly polarized light to that for linearly polarized light is approximately 1.4. These self-focusing studies are not yet complete and will be reported in detail at a later date. We emphasize that no data are included in this paper for which either the polarization test or the beam distortion test indicate the presence of self-focusing.

4. EXPERIMENTAL RESULTS AND DISCUSSIONS

Tables I through VIII summarize the results of measurements of the laser-induced breakdown thresholds for two different samples of single crystal NaCl and fused silica.* The NaCl sample labeled 78-NC-6 is the same sample used in previous picosecond damage studies[2] and in studies at long pulsewidths and wavelengths.[12,13] Both SiO_2 samples have been used in nanosecond studies at 1.06 μm,[14] and the sample labeled 79-FQ-125-1 was used in previous picosecond studies.[2] The uncertainties listed in the tables of data are the relative errors obtained by the method of Porteus et al.[15] The absolute errors, which include the relative errors and absolute errors in energy, pulsewidth, and focal spot radius, are estimated to be ±20% in the breakdown electric fields.

Tables I through IV summarize the results of our measurements at 0.53 μm for laser pulsewidths in the 25 to 200 ps (FWHM) range.

TABLE I. LID Data for Sample 79-FQ-7940-1 (SiO_2) at 0.53 μm*

W (μm)	t_p (ps)	I_B (TW/cm^2)	E_B (MV/cm)	P_B (MW)	ϵ_B (J/cm^2)
	25±4	1.32±0.13	18.3±0.9	1.07±0.11	35.0±3.5
7.2	53±5	0.78±0.08	14.1±0.7	0.64±0.06	44.0±4.4
	110±10	0.78±0.08	14.1±0.7	0.64±0.06	91±9
	37±5	1.40±0.14	18.9±0.9	0.55±0.06	55±6
5.0	105±15	1.20±0.12	17.5±0.8	0.47±0.05	134±13
	140±15	1.14±0.11	17.0±0.8	0.45±0.05	169±17
	180±20	1.10±0.11	16.7±0.7	0.43±0.04	210±21
	30±5	1.68±0.17	20.7±1.0	0.31±0.03	53±5
3.4	72±10	1.34±0.13	18.5±0.8	0.24±0.02	102±10
	105±15	1.07±0.11	16.5±0.8	0.19±0.02	83±8

*The error values listed are the relative uncertainties in the threshold for damage determined by the method used in Ref. 15. The absolute accuracy of these data and the data presented in the other tables is estimated to be ±20% in the breakdown field. In this table and those that follow, W = focal spot radius (HW $1/e^2$ M) in micrometers, t_p = laser pulsewidth (FWHM) in ps, I_B = breakdown irradiance, E_B = breakdown field, P_B = breakdown power, and ϵ_B = breakdown fluences.

TABLE II. LID Data for Sample 79-FQ-125-1 (SiO_2) at 0.53 μm*

W (μm)	t_p (ps)	I_B (TW/cm^2)	E_B (MV/cm)	P_B (MW)	ϵ_B (J/cm^2)
	25±4	0.96±0.10	15.7±0.8	0.79±0.08	25.5±3.0
7.2	105±15	0.48±0.05	11.0±0.5	0.39±0.04	53±5
	150±15	0.39±0.06	9.9±0.8	0.32±0.04	62±6
	34±4	1.02±0.10	16.1±0.8	0.40±0.04	37±4
5.0	120±15	0.86±0.09	14.8±0.7	0.34±0.03	109±11
	180±20	0.80±0.15	14.3±1.0	0.32±0.03	153±25
	32±4	1.16±0.15	17.2±1.0	0.21±0.02	39±4
3.4	120±15	0.91±0.09	15.2±0.5	0.16±0.02	115±12
	180±20	0.75±0.12	13.8±1.0	0.14±0.01	143±14

*See Table I for explanation of symbols and error bars.

TABLE III. LID Data for Sample 82-NC-1 (NaCl) at 0.53 μm*

W (μm)	t_p (ps)	I_B (GW/cm^2)	E_B (MV/cm)	P_B (kW)	ϵ_B (J/cm^2)
	35±4	57±6	3.80±0.25	174±17	2.10±0.20
14.0	80±8	35±4	2.98±0.15	107±10	2.96±0.30
	110±15	32±3	2.87±0.15	100±10	3.77±0.38
	41±9	91±9	4.80±0.35	120±12	3.95±0.40
7.2	82±7	64±6	4.03±0.19	40±4	5.50±0.60
	120±15	47±5	3.45±0.19	29±3	6.00±0.60
	26±4	139±14	5.95±0.48	26.0±0.3	3.83±0.38
	37±3	115±12	5.41±0.33	21.0±0.2	4.50±0.50
3.4	57±3	85±9	4.64±0.30	15.0±0.2	5.10±0.50
	73±4	71±7	4.24±0.52	12.8±0.12	5.50±0.60
	90±10	64±6	4.04±0.18	12.0±0.12	6.10±0.60
	115±15	35±4	3.00±0.31	6.4±0.64	4.30±0.40

*See Table I for explanation of symbols and error bars.

*The fused silica samples were acquired from Mark Optics, 1510 East St., Gertrude Road, Santa Ana, CA 92705. The SiO_2 designated 78-FQ-125-1 was a General Electric #125, high purity water-free sample, and the sample designated 79-FQ-7940-1 was a Corning #7940 sample which contained substantial water but was otherwise a high purity material. Both NaCl samples were single crystal "laser grade" material from the Harshaw Chemical Co., 6801 Cochran Road, Solon, OH 44139.

TABLE IV. LID Data for Sample 78-NC-6 (NaCl) at 0.53 μm*

W (μm)	t_p (ps)	I_B (GW/cm²)	E_B (MV/cm)	P_B (kW)	ϵ_B (J/cm²)
	25±5	120±12	5.53±0.33	370±40	3.19±0.32
14.0	105±15	48±5	3.50±0.20	148±15	5.37±0.54
	170±20	34±6	2.95±0.30	105±10	6.18±0.62
	30±5	148±15	6.14±0.30	120±12	4.72±0.47
7.2	105±15	50±5	3.55±0.20	40±4	5.53±0.56
	150±15	36±4	3.03±0.16	29±3	5.74±0.57
	28±4	184±18	6.86±0.31	33.0±3.3	5.48±0.55
	85±5	82±8	4.56±0.23	15.0±1.5	7.39±0.74
3.4	100±10	66±7	4.10±0.21	12.0±1.2	7.02±0.70
	120±10	55±8	3.75±0.30	10.0±1.0	7.05±0.71
	140±10	44±7	3.35±0.30	8.0±0.8	6.57±0.66
	170±20	34±5	2.95±0.21	6.0±0.6	6.17±0.62

*See Table I for explanation of symbols and error bars.

TABLE V. LID Data for Sample 79-FQ-7940-1 (SiO_2) at 1.05 μm*

W (μm)	t_p (ps)	I_B (TW/cm²)	E_B (MV/cm)	P_B (MW)	ϵ_B (J/cm²)
	7.9±0.6	1.12±0.11	16.8±0.8	3.44±0.34	9.4±0.9
	6.3±0.3	1.25±0.13	17.7±1.0	3.84±0.38	8.4±0.8
14.0	5.2±0.3	1.42±0.14	18.9±1.0	4.37±0.44	6.9±0.6
	3.6±0.3	1.75±0.18	21.0±1.1	5.39±0.54	6.7±0.7
	8.5±0.5	2.27±0.23	24.1±1.1	1.85±0.19	20.5±2.0
	7.5±0.5	2.20±0.22	23.7±1.1	1.79±0.18	17.5±1.8
7.2	6.5±0.5	2.60±0.26	25.7±1.3	2.12±0.21	18.0±1.8
	5.5±0.5	2.75±0.28	26.5±1.2	2.24±0.22	16.1±1.6
	4.5±0.5	3.14±0.31	28.3±1.3	2.56±0.26	15.0±1.5
	3.6±0.4	3.65±0.37	30.5±1.5	2.97±0.30	14.0±1.4
	8.5±0.5	3.04±0.30	27.8±1.4	1.19±0.12	27.6±2.8
	7.5±0.5	3.24±0.32	28.7±1.3	1.27±0.13	25.9±2.6
5.0	6.5±0.5	3.56±0.37	30.1±1.5	1.40±0.14	24.6±2.5
	5.5±0.5	3.94±0.39	31.7±1.5	1.55±0.16	23.1±2.3
	3.6±0.3	5.00±0.60	35.7±2.0	1.96±0.20	19.2±1.9

*See Table I for explanation of symbols and error bars.

These results will be compared here with the results of our earlier studies at 1.06 μm for these same materials over a similar range of pulsewidths. Tables V through VIII contain the results of measurements on these same samples at 1.05 μm for pulses in the 4 to 10 ps range. In addition, Tables VI and VIII contain LID thresholds at 1 μm in the pulsewidth range of 40 to 200 ps for a 7.2 μm focal spot radius. These thresholds are taken from Ref. 2 and were interpolated from measurements made at focal spot sizes of 6.1 and 10.3 μm. In subsequent measurements the LID thresholds for the 7.2 μm spot size were shown to be the same as the interpolated values within error bars.

In the paragraphs that follow, we examine the pulsewidth dependence of the threshold breakdown field E_B for a given sample at a given wavelength and focal spot radius. We then examine the wavelength dependence of E_B for a given pulsewidth and spot size.

The dependence of E_B on pulsewidth (t_p) is more clearly seen by plotting E_B versus the inverse pulsewidth on a log-log plot. Figures 3 and 4 are such plots for a SiO_2 sample (79-FQ-7940-1) and a NaCl sample (82-NC-1) at 1.05 μm. Note that for a given spot size and for pulses shorter than 10 ps the data for each sample can be fit with a straight line. Over this limited pulsewidth range

TABLE VI. LID Data for Sample 79-FQ-125-1 (SiO_2) at 1.05 μm*

W (μm)	t_p (ps)	I_B (TW/cm²)	E_B (MV/cm)	P_B (MW)	ϵ_B (J/cm²)
	9.5±0.5	0.88±0.09	15.0±0.7	2.71±0.27	5.01±0.50
	8.5±0.5	0.90±0.09	15.1±0.7	2.77±0.28	8.14±0.82
14.0	6.5±0.5	1.06±0.11	16.4±0.9	3.26±0.33	7.32±0.73
	4.0±0.5	1.8±0.20	21.4±1.2	5.54±0.56	7.66±0.77
	175±15	0.88±0.12	15.0±1.2	0.72±0.09	163±20
	92±15	0.92±0.13	15.3±1.1	0.75±0.10	90±12
	47±6	0.96±0.14	15.6±1.0	0.78±0.10	48±7
	9.5±0.5	1.93±0.19	22.1±1.1	1.57±0.16	19.5±2.0
7.2	7.5±0.5	2.05±0.21	22.8±1.2	1.67±0.17	16.3±1.6
	6.5±0.5	2.15±0.22	23.4±1.2	1.75±0.18	14.9±1.5
	5.5±0.5	2.30±0.23	24.2±1.2	1.87±0.19	13.5±1.4
	4.5±0.5	2.89±0.29	27.1±1.4	2.35±0.24	13.8±1.4
	3.5±0.6	3.31±0.33	29.0±1.4	2.69±0.27	12.3±1.2
	9.4±0.5	2.60±0.26	25.7±1.3	1.02±0.10	26.0±0.3
	7.5±0.5	3.26±0.33	28.8±1.4	1.28±0.13	26.0±0.3
5.0	6.5±0.5	3.77±0.38	31.0±1.5	1.45±0.15	26.1±0.3
	5.5±0.5	3.98±0.40	31.8±1.6	1.56±0.16	23.2±0.2
	4.5±0.5	4.49±0.45	33.8±1.6	1.76±0.18	21.5±0.2

*The data for 7.2 μm size and t_p = 47 to 175 ps are taken from Ref. 2 and are interpolated from measurements made at spot sizes of 6.1 and 10.3 μm and a laser wavelength of 1.06 μm. In subsequent measurements the LID thresholds for the 7.2 μm spot size were shown to be the same as the interpolated values within error bars. See Table I for explanation of symbols and error bars.

TABLE VII. LID Data for Sample 82-NC-1 (NaCl) at 1.05 μm*

W (μm)	t_p (ps)	I_B (TW/cm²)	E_B (MV/cm)	P_B (MW)	ϵ_B (J/cm²)
	9.5±0.5	0.25±0.03	8.00±0.44	0.77±0.08	2.55±0.26
	8.5±0.5	0.26±0.03	8.18±0.41	0.81±0.08	2.38±0.24
14.0	7.5±0.5	0.29±0.03	8.60±0.43	0.89±0.09	2.31±0.23
	6.5±0.5	0.37±0.04	9.64±0.57	1.12±0.11	2.55±0.26
	5.5±0.5	0.40±0.04	10.10±0.48	1.23±0.12	2.38±0.24
	4.5±0.5	0.45±0.05	10.70±0.58	1.37±0.14	2.12±0.21
	7.5±0.5	0.66±0.07	12.9±0.73	0.53±0.05	5.22±0.52
	6.5±0.5	0.75±0.08	13.8±0.73	0.61±0.06	5.15±0.52
7.2	5.5±0.5	0.88±0.09	14.9±0.81	0.71±0.07	5.12±0.52
	4.5±0.5	0.97±0.10	15.7±0.80	0.79±0.08	4.65±0.47
	3.6±0.3	1.38±0.14	18.8±0.87	1.12±0.09	5.28±0.53
	7.5±0.5	0.74±0.07	13.7±0.65	0.29±0.03	5.86±0.59
5.0	6.5±0.5	1.00±0.10	15.9±0.83	0.39±0.04	6.91±0.69
	5.5±0.5	1.14±0.11	17.0±0.83	0.45±0.05	6.66±0.67
	4.5±0.5	1.29±0.13	18.1±0.91	0.51±0.05	6.20±0.62

*See Table I for explanation of symbols and error bars.

$$E_B \propto t_p^{-x}, \tag{2}$$

where $x \doteq 0.3$ for the SiO_2 sample and $x \doteq 0.5$ for the NaCl sample. The displacement of each set of data points corresponding to different focal spot sizes indicates a relatively strong spot size dependence in these samples at this wavelength.

Figures 5 and 6 are similar plots for the same two samples (79-FQ-7940-1 and 82-NC-1) at 0.53 μm for pulsewidths in the 25 to 200 ps range. Again one can fit the data with a linear dependence. However, in this case $x < 0.1$ for the SiO_2 sample and $x \doteq 0.3$ for the NaCl sample. Similar trends are seen in the data for the other SiO_2

TABLE VIII. LID Data for Sample 78-NC-1 (NaCl) at 1.05 μm*

W (μm)	t_p (ps)	I_B (TW/cm^2)	E_B (MV/cm)	P_B (MW)	ϵ_B (J/cm^2)
	7.5 ± 0.5	0.26 ± 0.03	8.06 ± 0.54	0.79 ± 0.08	2.03 ± 0.20
14.0	6.5 ± 0.5	0.28 ± 0.03	8.44 ± 0.44	0.86 ± 0.09	1.95 ± 0.20
	5.5 ± 0.5	0.32 ± 0.03	9.03 ± 0.44	0.99 ± 0.10	1.87 ± 0.19
	4.5 ± 0.5	0.38 ± 0.04	9.80 ± 0.53	1.17 ± 0.12	1.82 ± 0.18
	167 ± 16	0.083 ± 0.011	4.6 ± 0.3	0.068 ± 0.008	14 ± 1.5
	100 ± 10	0.110 ± 0.008	5.1 ± 0.4	0.090 ± 0.006	11.7 ± 1.2
	45 ± 3	0.118 ± 0.018	5.5 ± 0.4	0.096 ± 0.010	5.56 ± 0.60
7.2	6.5 ± 0.5	0.58 ± 0.06	12.2 ± 0.6	0.43 ± 0.04	4.00 ± 0.40
	5.5 ± 0.5	0.66 ± 0.07	12.9 ± 0.73	0.53 ± 0.05	3.83 ± 0.38
	4.5 ± 0.5	0.80 ± 0.08	14.3 ± 0.63	0.65 ± 0.07	3.83 ± 0.38
	3.5 ± 0.5	0.95 ± 0.10	15.6 ± 0.64	0.77 ± 0.08	3.56 ± 0.36
	7.5 ± 0.5	0.92 ± 0.09	15.3 ± 0.73	0.36 ± 0.04	7.30 ± 0.73
	6.5 ± 0.5	0.94 ± 0.09	15.5 ± 0.69	0.37 ± 0.04	6.53 ± 0.65
5.0	5.5 ± 0.5	1.13 ± 0.11	17.0 ± 0.76	0.44 ± 0.04	6.62 ± 0.66
	4.5 ± 0.5	1.20 ± 0.12	17.5 ± 0.83	0.47 ± 0.05	5.78 ± 0.58
	3.4 ± 0.1	1.60 ± 0.16	20.2 ± 0.94	0.63 ± 0.06	5.78 ± 0.58

*The data for 7.2 μm size and t_p = 45 to 167 ps are taken from Ref. 2 and are interpolated from measurements made at spot sizes of 6.1 and 10.3 μm and a laser wavelength of 1.06 μm. In subsequent measurements the LID thresholds for the 7.2 μm spot size were shown to be the same as the interpolated values within error bars. See Table I for explanation of symbols and error bars.

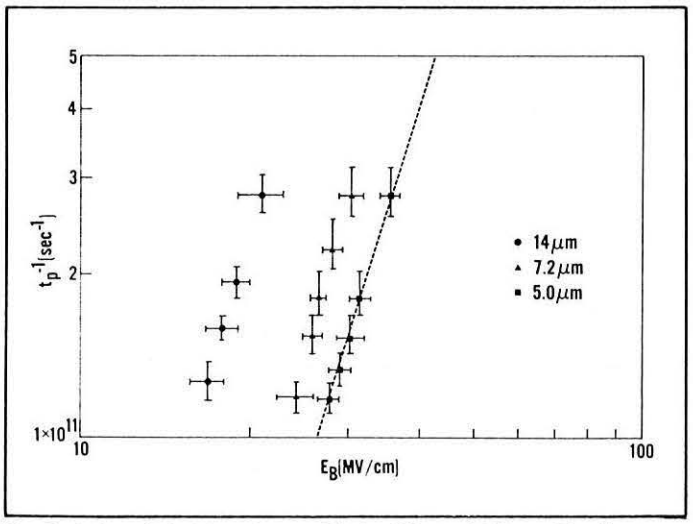

Fig. 3. Pulsewidth dependence of E_B for SiO_2 at 1.05 μm. The three sets of points correspond to different focal spot radii, and the relatively large displacement of the three sets of points is indicative of a large spot size dependence in the damage threshold. The slope of the least square fit for each set of points is approximately 0.3 for this pulsewidth range ($t_p < 10$ ps).

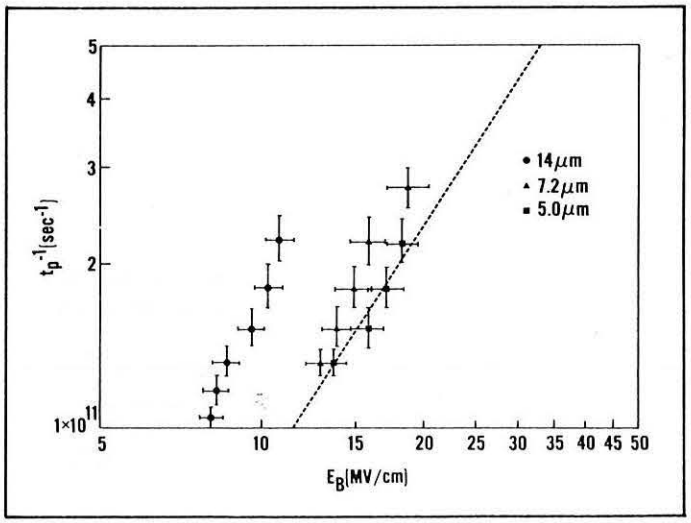

Fig. 4. Pulsewidth dependence of E_B in NaCl at 1.05 μm. The slope of the least square linear fit to each of the three sets of points is approximately 0.5. This indicates an inverse square root of pulsewidth dependence of E_B for this pulsewidth range ($t_p < 10$ ps).

and NaCl samples given in Tables II, IV, VI, and VIII.

At 0.53 μm and 1.06 μm the pulsewidth dependence of E_B observed for both materials is in good agreement with the predictions of various avalanche breakdown models.[16–18] For example, the model proposed by Sparks et al.[16] predicts very little pulsewidth dependence for relatively long pulses (ns) and a dependence of E_B on pulsewidth which approaches an inverse square root dependence for relatively short pulses, i.e., tens of picoseconds. The inverse square root of pulsewidth dependence implies that the breakdown fluence is constant (as can be seen in Tables VII and VIII for the NaCl samples). We find that for NaCl in the long pulsewidth limit ($t_p > 1$ ns)[2] the breakdown *field* is nearly constant, whereas in the short pulsewidth limit ($t_p < 10$ ps) the breakdown *fluence* is nearly constant. The trend in the t_p dependence of E_B for SiO_2 is similar to that seen in NaCl; however, the strongest dependence of E_B on t_p observed was $E_B \propto t_p^{-0.3}$ for pulses shorter than 10 ps at 1.05 μm. It is important to note that the strongest pulsewidth dependence of E_B observed in these measurements was the approximate inverse square root of pulsewidth dependence observed for NaCl for $t_p < 10$ ps at 1.05 μm. In an avalanche breakdown model this dependence implies an ionization rate (β) which is proportional to the input irradiance. Then, the buildup of carriers is given by[16]

$$N = N_o e^{\beta t} = N_o e^{AE^2 t}, \quad (3)$$

where N is the carrier density, N_o is the initial carrier density or carrier density produced by multiphoton ionization, and A is a constant. It is commonly assumed that damage occurs when the

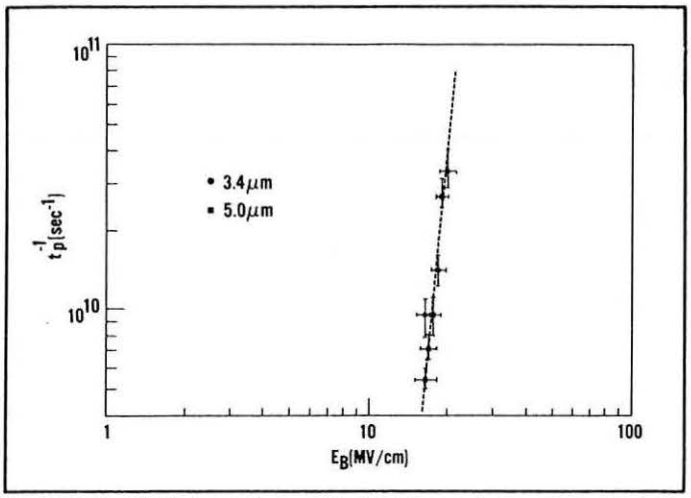

Fig. 5. Pulsewidth dependence of E_B in SiO_2 at 0.53 μm. Note that E_B is nearly independent of t_p in this pulsewidth range (20 to 200 ps) and that there is little spot size dependence in E_B for the two spot sizes shown (3.4 and 5.0 μm).

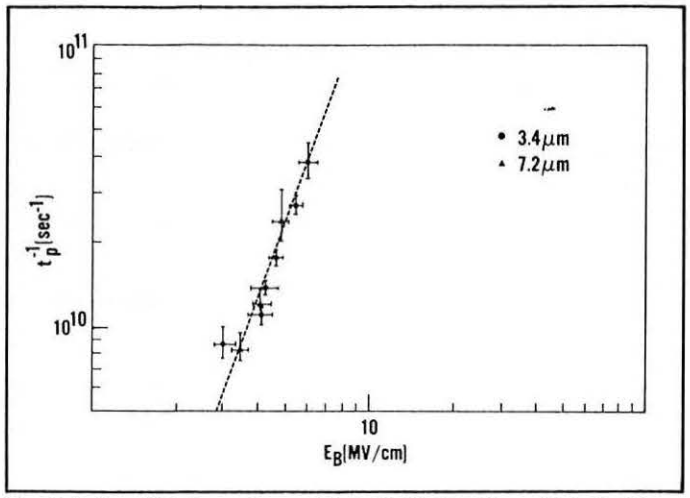

Fig. 6. Pulsewidth dependence of E_B in NaCl at 0.53 μm. Note that there is little spot size dependence in E_B for the two spot sizes shown (3.4 and 7.2 μm). The least squares linear fit of these data give a slope of 0.3, or nearly an inverse fourth root dependence of E_B on t_p for pulsewidths in this range (20 to 200 ps).

carrier density reaches a critical value N_c. Thus, Eq. (3) gives the following relationship for E_B:

$$E_B = \left(1/\sqrt{t_p}\right) \left\{\left[\ell n(N_c/N_o)\right]/A\right\}^{1/2}, \quad (4)$$

and the { } term is constant for a given sample and laser frequency. The breakdown fluence ϵ_B is proportional to E_B^2 times the laser pulsewidth. Therefore, Eq. (4) implies that ϵ_B is a constant for β proportional to E^2.

In the Sparks' avalanche breakdown model, the ionization rate β is proportional to E^2 in the high electric field limit. This limit corresponds to the situation in which the increase in energy of the electrons in the conduction band is simply proportional to the input irradiance and in which all losses are negligible. This simply says that the ionization rate is limited by the rate at which the input light beam can supply energy to the conduction band electrons. For the low field limit, i.e., longer pulses, β is exponentially dependent on E and the resulting pulsewidth dependence is relatively weak.

Other workers have used an approximate inverse pulsewidth dependence [i.e., x = 1 in Eq. (2)] to scale breakdown data for various materials.[19,20] This is a much stronger dependence than is observed in this work. Their strong pulsewidth dependence was determined by combining the 1.06 μm, 30 ps data in Ref. 20, and the 1.06 μm, 15 ps data in Ref. 21. These two data points were taken with different focal spot sizes. That is, the 30 ps data point in Ref. 20 was taken with relatively small focal radii (4.7 to 5.9 μm $1/e^2$ radius) and was reduced with the assumption that self-focusing was dominating the observed damage. The 15 ps data point in Ref. 21 was taken with a relatively large focal radius (12.4 μm HW $1/e^2$ M), and thus higher input power. In the latter work the authors assumed that self-focusing was not present in their experiment. The relatively large pulsewidth dependence deduced from these two isolated data points is probably due to differences in experimental conditions used in the two measurements and the different methods of data reduction.

We now examine the wavelength dependence of the breakdown thresholds for laser pulsewidths in the 25 to 200 ps range. In Fig. 7 we have plotted, in bar graph form, the breakdown electric fields for SiO_2 (sample 79-FQ-125-1) and NaCl (sample 78-NC-6) for 1.06 μm and 0.53 μm for various pulsewidths at a fixed focal spot radius (7.2 μm). The 1.06 μm LID thresholds at the 7.2 μm focal radius are taken from Ref. 2 and are interpolated from measurements at spot sizes of 6.1 and 10.3 μm. In subsequent measurements the LID thresholds for the 7.2 μm spot size were shown to be the same as the interpolated values within error bars. In two cases where the pulsewidths did not exactly overlap for the two wavelengths we interpolated the 0.53 μm

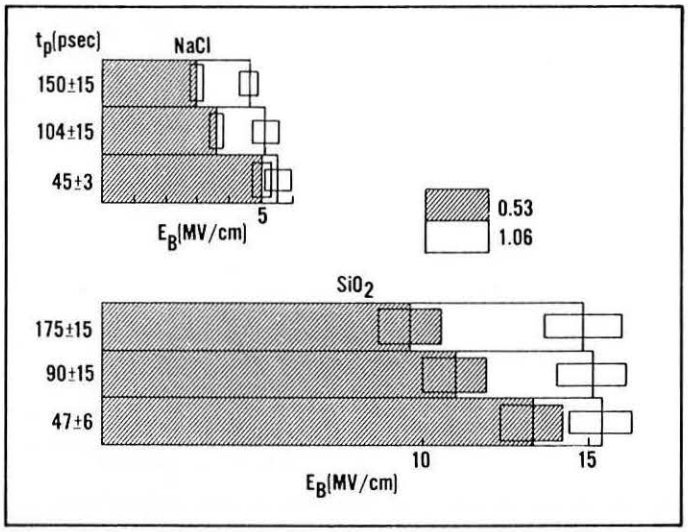

Fig. 7. Wavelength dependence of the breakdown field E_B for NaCl and SiO_2 for a variety of laser pulsewidths. All the above data were taken on the same sample of NaCl and the same sample of SiO_2. The 1.06 μm thresholds are taken from Ref. 2 and are interpolated from measurements made at spot sizes 6.1 and 10.3 μm. In subsequent measurements the LID thresholds for the 7.2 μm spot size were shown to be the same as the interpolated values within error bars.

data between two pulsewidths for which data was available. This procedure was made necessary by the fact that only a limited number of pulsewidths were available at each wavelength studied. The errors due to interpolation are estimated to be within the error bars shown in Fig. 7.

Note that for each pulsewidth range plotted in Fig. 7, the breakdown field is less at 0.53 μm than at 1.06 μm for both the SiO_2 and the NaCl samples. In recent preliminary measurements this trend was also observed for pulses shorter than 10 ps. Avalanche breakdown theory predicts an increase in E_B with decreasing wavelength, which is clearly inconsistent with the results shown in Fig. 7. The observed decrease in breakdown field with wavelength, while in the right direction, is much too weak for a strictly multiphoton process. One possible explanation for these results is a multiphoton-initiated avalanche breakdown model, which has been previously suggested.

Smith et al.[19] observed an increase in the breakdown threshold

with decreasing wavelength for picosecond pulses. However, the data presented in that work were scaled for the presumed effects of self-focusing over a range of pulsewidths and spot sizes in which we observe no such effects. In addition, it is unclear whether the same samples were used in the wavelength comparison. Manenkov[22] observed an initial increase in the damage threshold for a sample of NaCl from 1.06 μm to 0.69 μm, then a decrease in the damage threshold at 0.53 μm for pulses ranging from 15 to 8 ns. The data presented in that work were not scaled for self-focusing.

5. SUMMARY

Laser-induced breakdown was studied as a function of pulsewidth and wavelength for a variety of focal conditions in fused SiO_2 and single crystal NaCl. Beam quality measurements and polarization dependence studies indicated the absence of self-focusing effects for the focusing conditions used in these experiments such that no self-focusing corrections need be used.

For the two materials studied, the breakdown field (E_B) increases with decreasing pulsewidth. The observed pulsewidth dependence for a given spot size and wavelength is consistent with the pulsewidth dependence predicted by various electron avalanche breakdown models. However, the spot size dependence observed in this study is not predicted by any avalanche theory, and is probably due to the extrinsic nature of the observed damage. Differences in LID thresholds for different samples of the same material seen in the data presented are further evidence that extrinsic properties influence the observed damage. The strongest pulsewidth dependence observed was in NaCl at 1.05 μm for pulses shorter than 10 ps. For these short pulses E_B increases as the inverse square root of the pulsewidth, indicating that the breakdown fluence is constant.

For conditions of equal pulsewidth and the same focal spot size, i.e., pulsewidths from 45 to 175 ps and a focal radius of 7.2 μm, E_B is less at 0.53 μm than at 1.06 μm for both materials. Avalanche breakdown theories predict an *increase* in E_B for shorter wavelengths. The observed *decrease* in breakdown field with wavelength, while in the right direction is much too weak for a strictly multiphoton process. One possible explanation for these results is that damage is due to a multiphoton-initiated avalanche breakdown process. In such a process electrons are excited to the conduction band by multiphoton excitation of impurities or defect states within the material band gap (i.e., extrinsic effects). After a few electrons are present in the conduction band, avalanche ionization takes over and dominates the damage process. Thus, the freqency dependence observed may be partly due to the multiphoton initiation process and the pulsewidth dependence indicative of an avalanche ionization process.

6. ACKNOWLEDGMENTS

The authors acknowledge the support of the Office of Naval Research, the National Science Foundation, The Robert A. Welch Foundation, and the North Texas State University Faculty Research Fund.

7. REFERENCES

1. A central depository of work in this area is the proceedings of the symposium on Laser-Induced Damage in Optical Materials, National Bureau of Standards (U.S.) Special Publications #341 (1970), #356 (1971), #372 (1972), #387 (1973), #414 (1974), #435 (1975), #462 (1976), #509 (1977), #541 (1978), #568 (1979), #620 (1980). These may be obtained from the Superintendent of Documents, U.S. Government Printing Office, Washington, DC 20402. Papers in these proceedings contain further reference to materials in this field.
2. E. W. Van Stryland, M. J. Soileau, Arthur L. Smirl, and William E. Williams, Phys. Rev. B 23, 2144(1981).
3. A. L. Smirl, T. F. Boggess, B. S. Wherrett, G. P. Perryman, and A. Miller, IEEE J. Quantum Electron. QE-19, 690(1983).
4. E. W. Van Stryland, W. E. Williams, M. J. Soileau, and A. L. Smirl, 1981 Conf. on Laser-Induced Damage in Optical Materials, (to be published by Natl. Bur. Stand.).
5. Y. R. Shen, Phys. Rev. Lett. 20, 378(1966).
6. A. Feldman, D. Horowitz, and R. Waxler, Natl. Bur. Stand. (U.S.) Spec. Publ. 372, 92(1972).
7. C. C. Wang, Phys. Rev. 152, 149(1966).
8. R. W. Hellworth, *Progress in Quantum Electronics,* Vol. 5, pp. 1–68, Pergamon Press, New York (1977).
9. M. J. Soileau, W. E. Williams, E. W. Van Stryland, and S. F. Brown, Proc. 1981 Conf. on Laser-Induced Damage in Optical Materials (to be published by Natl. Bur. Stand.).
10. D. H. Close, C. R. Giuliano, R. W. Hellworth, L. D. Hess, F. J. McClung, and W. G. Wagner, IEEE J. Quantum Electron. QE-2, 553(1966).
11. E. W. Van Stryland, A. L. Smirl, T. F. Boggess, and F. A. Hopf, in *Picosecond Phenomena III,* p. 368, Springer-Verlag, New York (1982).
12. M. J. Soileau, Ph.D. Thesis, University of Southern California, 1979 (unpublished).
13. M. J. Soileau and M. Bass, and P. H. Klein, Natl. Bur. Stand. (U.S.) Spec. Publ. 568, 497(1979).
14. M. J. Soileau and M. Bass, IEEE J. Quantum Electron. QE-16, 814(1980).
15. J. O. Porteus, J. L. Jernigan, and W. N. Faith, Natl. Bur. Stand (U.S.) Spec. Publ. 509, 507(1977).
16. M. Sparks, T. Holstein, R. Warren, D. L. Mills, A. A. Maradudin, L. J. Shan, E. Loh, Jr., and F. King, Natl. Bur. Stand. (U.S.) Spec. Publ. 568, 467(1979).
17. S. Brawer, Phys. Rev. B 20, 3422(1979).
18. A. S. Epifanov, IEEE J. Quantum Electron. QE-17, 2018(1981).
19. W. L. Smith, J. H. Bechtel, and N. Bloembergen, Phys. Rev. B 15, 4039(1977).
20. W. Lee Smith, J. H. Bechtel, and N. Bloembergen, Phys. Rev. B 12, 706(1975).
21. D. W. Fradin, N. Bloembergen, and J. P. Lettlier, Appl. Phys. Lett. 22, 635(1973).
22. A. A. Manekov, Natl. Bur. Stand. (U.S.) Spec. Publ. 509, 455(1977). ∞